Electronic structure, lattice dynamics, and magnetic properties of Th*X*AsN (*X* = Fe, Co, Ni) superconductors: A first-principles study

Smritijit Sen[1] and Guang-Yu Guo[1,2,*]

[1]*Department of Physics and Center for Theoretical Physics, National Taiwan University, Taipei 10617, Taiwan, Republic of China*
[2]*Physics Division, National Center for Theoretical Sciences, Hsinchu 30013, Taiwan, Republic of China*

In this work, we present a comparative first-principles study of the mechanical properties, electronic structure, phonon dispersion relation, electron-phonon coupling, and magnetism in three isostructural superconductors, namely ThFeAsN, ThCoAsN, and ThNiAsN. Experimentally, ThFeAsN and ThNiAsN show superconducting properties, while ThCoAsN has not been synthesized. Our calculated elastic constants show that all these systems are mechanically stable. Significant differences in the electronic structures of these three compounds in terms of density of states, band structures, and Fermi surfaces are found. Our phonon calculations reveal that all the systems, including ThCoAsN, are dynamically stable. Phonon dispersion relations indicate that the optical modes of all three systems are almost the same, while there are significant variations in the low-frequency manifold consisting of mixed modes. The electron-phonon coupling constants and superconducting transition temperatures calculated based on the Eliashberg formalism predict a rather high T_c of 6.4 K for ThCoAsN and also a T_c of 3.4 K for ThNiAsN, which agrees well with the experimental value of 4.3 K. Nevertheless, we find a T_c of 0.05 K for ThFeAsN, which is much smaller than the experimental T_c of $\sim$30 K. However, a simple analysis considering the amplifying effects of spin density wave order and out-of-plane soft phonon modes suggests that the T_c could be increased considerably to $\sim$10 K. Finally, we also discuss the effect of anion As height on the electronic structures, and we study possible magnetic states in these three compounds.

I. INTRODUCTION

Since the discovery of high-temperature superconductivity in LaFeAs(O, F) [1], a large number of new Fe-based superconductors (SCs), popularly known as pnictides, have been found. Most of the Fe-based SCs are generally categorized into six families depending upon their chemical compositions, namely 11, 111, 122, 122*, 1111, and 42622 (some times denoted as 21311) [2]. Interestingly, two newly discovered families 112 and 1144 also show some unique features that are not of the usual characteristics of Fe-based SCs [3,4]. All these systems have a tetragonal crystal structure with the FeAs/FeSe layers as the basic building blocks, which seem to play an important role in superconductivity. Along with these Fe-based SCs, some isostructural Ni/Co-based systems with or without superconducting properties have also been reported [5–8]. For example, LaNiAsO, a 1111-type nickel-based pnictide, was reported to become superconducting below a temperature of 2.75 K [6]. On the other hand, LaCoAsO was found to be a ferromagnet with no trace of superconductivity [9]. Similarly, BaCo$_2$As$_2$, which is isostructural to Fe-based superconductor BaFe$_2$As$_2$, was also reported to be nonsuperconducting [10].

Apart from its unconventional superconducting property, Fe-based SCs display a number of exotic normal state properties such as spin density wave (SDW), orbital density wave (ODW), structural phase transition, and nematic order,

which are distinctly different from other classes of high superconducting transition temperature (T_c) SCs including cuprates [11–15]. Although nickel-based pnictides possess the same crystal structure as that of the Fe-pnictides, the superconducting pairing mechanism in these systems may be quite different from that of the Fe-based SCs. In particular, T_c of nickel-based pnictides can be calculated rather accurately within the Eliashberg formalism of the electron-phonon coupling mediated superconductivity [16,17] (see also Sec. III D below). Recent studies show that the role of electron-phonon coupling in Fe-based SCs has been understated especially in the presence of SDW-type antiferromagnetic order [18–20].

Being multiorbital in nature, Fermi surface topology of Fe-based SCs is quite different from other high-T_c SCs, and it is sensitive to temperature, pressure, and impurity doping. A sign-changing $s^{\pm}$ superconducting order parameter is widely accepted for describing various physical properties of Fe-based SCs [21], but there is strong evidence of deviation of the $s^{\pm}$ pairing scenario [22]. Therefore, the pairing symmetry of these SCs is still under considerable debate [22–24]. In general, Fe-based SCs have high critical current density as well as high upper critical magnetic field (H_{c2}). Added to that, they possess moderate anisotropy (important for transport of charge) and ductility, which give these SCs an edge over high-T_c cuprates as far as superconducting applications are concerned [25]. These Fe-based SCs have all the potential to be the next-generation SCs. Therefore, a better theoretical understanding of these systems will accelerate the development of more sophisticated technologies based on pnictide SCs.

---

*Corresponding author: gyguo@phys.ntu.edu.tw

Superconductivity in the stoichiometric ThFeAsN compound in ambient pressure with a remarkably high T_c of 30 K was recently reported [26]. This new 1111-type FeAs based compound with a ZrCuSiAs-type structure, where the (LaO) layers in LaOFeAs are replaced by the ThN layers. Unlike ReFeAsO series, this newly discovered Fe-based SC does not show any long-range magnetic order. However, evidence of strong magnetic fluctuations above 35 K was found via muon-spin rotation/relaxation and nuclear magnetic resonance techniques [27]. ThFeAsN has a distinctively shorter c-axis (the a-axis is similar) as compared to the LaFeAsO series of Fe-based SCs. This suggests that ThFeAsN possesses an in-built uniaxial chemical pressure along the c-axis which has a significant impact on the physical properties observed in these compounds. The advent of superconductivity in ThFeAsN, without intrinsic doping or external pressure, and in the absence of long-range magnetic order, makes this system quite unique as compared to the other 1111 FeAs-based SCs. Therefore, study of the low-energy electronic structure of ThFeAsN will provide a wealth of information.

The recent discovery of room-temperature superconductivity in a number of compounds including solidified H_2S under hydrostatic pressure, and its close proximity to electron phonon couplings, challenges the general consensus of high-temperature superconductivity [28,29]. It is also shown that superconductivity in the structurally similar compound ThNiAsN is phonon-mediated, and the superconducting transition temperature estimated from density functional perturbation theory calculations within the Eliashberg formalism is 3.5 K, which agrees well with the experimentally measured T_c of 4.3 K [30,31]. Therefore, it is important to study the role of electron-phonon coupling in the superconductivity of ThFeAsN.

A recent first-principles investigation of ThFeAsN reveals a stripe antiferromagnetic (AF) ground state, contrary to the experimental ground state with no long-range magnetic order [32,33]. Recent theoretical studies, which include the effect of SDW-type AF orders on electron-phonon coupling for various Fe-based SCs such as FeSe and LiFeAs, were able to explain the experimental T_c of these systems as well as its pressure dependence [34]. From these works, it is quite evident that one should consider the combined effect of the AF order and soft out-of-plane lattice vibration on electron-phonon coupling to understand the observed T_c. Recent electronic structure calculations also disclose that ThFeAsN is a semimetal and possesses partially nested electron and hole Fermi surface pockets [35]. On the other hand, the latest theoretical studies [31] indicate that ThNiAsN possesses a quite different electronic structure from that of ThFeAsN with no magnetic ordering. In this work, we also study the mechanical properties, electronic structure, and lattice dynamics of the isostructural compound ThCoAsN. A comparative study of ThXAsN (X = Fe,Co,Ni) will help to elucidate the mechanism of superconductivity in these compounds, and this is the main goal of this paper.

The rest of this paper is organized as follows. In the next section, we briefly describe the crystalline structure of ThXAsN (X = Fe,Co,Ni) and also the details of our first-principles calculations. In Sec. III A, we first calculate the elastic constants of ThXAsN (X = Fe,Co,Ni), which show
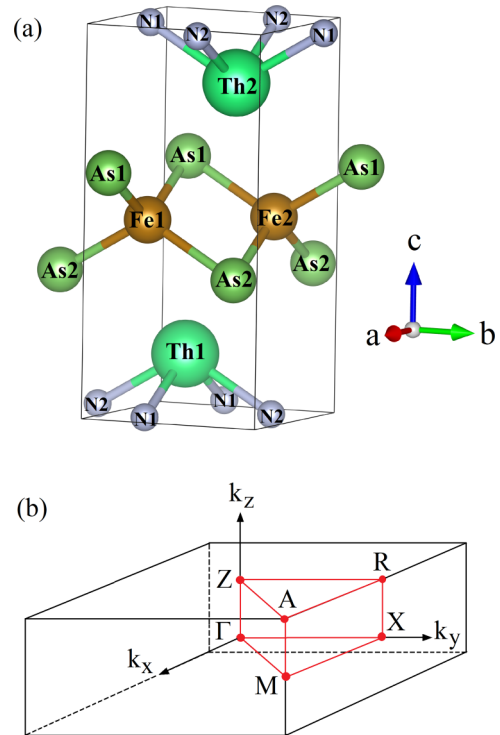

FIG. 1. (a) Crystal structure and (b) Brillouin zone of ThFeAsN. ThNiAsN, and ThCoAsN possess the same crystal structure with Fe atoms being replaced by Ni and Co atoms, respectively.

that these systems are mechanically stable. We also discuss some of the important mechanical properties of these systems from an application point of view. In addition, we evaluate the plasma frequencies of the systems along different axes to understand the effective dimensionality of these systems, and we compare these values with other Fe-based SCs in Sec. III B. Next we report the calculated electronic structures of ThXAsN (X = Fe,Co,Ni), especially the density of states (DOS), band structure, and Fermi surface in Sec. III C. Then, in Sec. III D, we present the calculated phonon dispersion relations and electron-phonon coupling for ThXAsN (X = Fe,Co,Ni). We also evaluate superconducting transition temperatures of these compounds within the Eliashberg theory. In Sec. IV, we study possible magnetic states in these systems. We also discuss the possible amplification of the electron-phonon coupling strength in the presence of AF order in ThFeAsN. Finally, we examine the influence of anion As height on the low-energy electronic structure, especially the Fermi surface of ThFeAsN. In Sec. V, the conclusions drawn from this work are summarized.

II. CRYSTAL STRUCTURE AND COMPUTATIONAL METHODS

All three considered ThXAsN (X = Fe,Co,Ni) compounds have the same tetragonal symmetry with space group $P4/nmm$ (No. 129) and contain two formulas units (f.u.) per unit cell, as illustrated in Fig. 1. Our first-principles structural optimization as well as electronic structure, mechanical, and lattice dynamical property calculations are based on the density functional theory with the generalized-gradient approximation

TABLE I. Lattice constants (a, c) as well as theoretical atomic fractional z coordinates and anion As height (h_{As}) of ThXAsN (X = Fe,Co,Ni). For ThFeAsN and ThNiAsN, the experimental lattice constants are used. For ThCoAsN, lattice constants are also determined theoretically (see Sec. II).

	a	c	z_{As}	z_{Th}	h_{As} (Å)
ThFeAsN	4.0414[a]	8.5152[a]	0.6388	0.1382	1.18
ThCoAsN	4.0570	8.3519	0.6404	0.1377	1.17
ThNiAsN	4.0804[b]	7.9888[b]	0.6405	0.1396	1.12

[a]Reference [40].
[b]Reference [30].

(GGA) to the exchange-correlation potential [36]. For the structural optimization, electronic structure, and elastic constant calculations, the accurate projector-augmented wave (PAW) method, as implemented in the Vienna *ab-initio* simulation package (VASP) [37–39], is used. The wave functions are expanded in the plane-wave basis with a large energy cutoff of 600 eV. The Brillouin zone integration is performed using a Γ-centered $10 \times 10 \times 5$ Monkhorst-Pack grid. For the Fermi surface calculations, a denser k-point grid of $20 \times 20 \times 20$ is chosen. In the structural optimizations, the atomic positions are relaxed until the atomic forces are less than 0.0001 eV/Å. In the self-consistent total energy and electronic structure calculations, an energy convergence of 10^{-6} eV is adopted,

The available experimental lattice constants of ThFeAsN [40] and ThNiAsN [30] (see Table I) are used, whereas the atomic positions are determined theoretically by our structural optimization, as described above. Since ThCoAsN has not been prepared experimentally, both lattice constants and atomic positions are determined theoretically. In all these structural optimization calculations, the nonmagnetic (NM) state is assumed unless stated otherwise. The lattice constants and atomic positions of all three systems used in the present calculations of the elastic constant, electronic structure, and lattice dynamics are listed in Table I.

The elastic constants of the ThXAsN compounds are determined by using the linear-response stress-strain method, as implemented in the VASP code [41]. Under a small strain (ϵ_{kl}), according to Hooke's law, the corresponding stress (σ_{ij}) can be written as $\sigma_{ij} = C_{ijkl}\epsilon_{kl}$, where C_{ijkl} is the stiffness tensor, which consists of the elastic constants of the crystal. The total number of independent elastic constants depends on the crystal symmetry. For example, a cubic crystal has only three independent elastic constants of C_{11}, C_{12}, and C_{44} [42,43]. On the other hand, the present ThXAsN systems with tetragonal symmetry have six independent elastic constants, namely C_{11}, C_{12}, C_{13}, C_{33}, C_{44}, and C_{66} [42–44].

Within the Voigt-Reuss-Hill (VRH) approximation [45], the macroscopic bulk moduli (B) and shear moduli (G) of a polycrystalline material can be estimated using the elastic constants of the single crystal mentioned in the preceding paragraph, as $B = (B_v + B_R)/2$ and $G = (G_v + G_R)/2$. Here $B_v = \frac{1}{9}\{2(C_{11} + C_{12}) + C_{33} + 4C_{13}\}$ and $G_v = \frac{1}{15}\{2C_{11} - 1C_{12} + C_{33} - 2C_{13} + 6C_{44} + 3C_{66}\}$ are the minimum bulk moduli and shear moduli of the single crystal, respectively. $B_R = \{C_{33}(C_{11} + C_{12}) - 2C_{13}^2\}/\{C_{11} + C_{12} + 2C_{33} - 4C_{13}\}$ and $G_R = 15/\{18B_v/C^2 + 6/(C_{11} - C_{12}) + 6/C_{44} + 3/C_{66}\}$

are the maximum bulk moduli and shear moduli of the single crystal, respectively. Furthermore, Young's modulus (Y) and Poisson's ratio (ν) of the polycrystalline material can be written in terms of B and G as $Y = 9BG/(3B + G)$ and $\nu = (3B - 2G)/2(3B + G)$. The averaged sound wave velocity of the polycrystalline material can be written as [46] $\overline{v}_m = [\frac{1}{3}(\frac{2}{\overline{v}_t^3} + \frac{1}{\overline{v}_l^3})]^{-1/3}$, where $\overline{v}_l$ and $\overline{v}_t$ are the averaged longitudinal and transverse elastic wave velocities, respectively, which are related to B and G as $\overline{v}_l = (\frac{B+4G/3}{\rho})^{1/2}$ and $\overline{v}_t = (\frac{G}{\rho})^{1/2}$. Finally, the Debye temperature of the polycrystalline material can be estimated from the average sound wave velocity via [46]

$$\Theta_D = \frac{h}{k_B}\left[\frac{3n}{4\pi}\left(\frac{N_A\rho}{M}\right)\right]^{1/3}\overline{v}_m, \tag{1}$$

where h is Planck's constant, k_B is Boltzmann's constant, N_A is Avogadro's number, ρ is the density, M is the molecular weight, and n is the number of atoms per unit cell.

All the phonon and electron-phonon coupling calculations are performed using the plane-wave pseudopotential method, as implemented in the QUANTUM ESPRESSO package [47]. All the pseudopotentials are taken from the Pslibrary [48]. The phonon dispersions and electron-phonon coupling are calculated based on the first-principles density functional perturbation theory (DFPT) [49]. We choose the plane-wave energy cutoff as 55 Ry and the charge density cutoff as 220 Ry. A Gaussian broadening method with the Gaussian width of 0.02 Ry is used in the Brillouin zone integration. A k-mesh of $12 \times 12 \times 6$ for electrons and a q-mesh of $6 \times 6 \times 3$ for phonons are used for all three systems. The electron-phonon coupling constant (λ) can be evaluated using the relation [50,51]

$$\lambda = 2\int\frac{\alpha^2F(\omega)}{\omega}d\omega, \tag{2}$$

where the Eliashberg spectral function

$$\alpha^2F(\omega) = \frac{1}{2\pi N(E_F)}\sum\frac{\gamma_{qj}}{\omega_{qj}}\delta(\hbar\omega - \hbar\omega_{qj}). \tag{3}$$

Here $N(E_F)$ is the electronic density of states at the Fermi level (E_F), γ_{qj} is the phonon linewidth due to electron-phonon scattering, and ω_{qj} is the phonon frequency with wave vector q and branch index j. Finally, the phonon-mediated superconducting transition temperature in Kelvin can be evaluated using the Allen and Dynes-modified McMillan's formula [50,51]:

$$T_c = \frac{\omega_{\log}}{1.2}\exp\left[\frac{-1.04(1 + \lambda)}{\lambda - \mu^*(1 + 0.62\lambda)}\right], \tag{4}$$

where $\omega_{\log}$ is the logarithmic average phonon frequency, and μ^* is the averaged screened electron-electron interaction.

III. NONMAGNETIC STATE PROPERTIES

In this section, we present the calculated physical properties of ThXAsN (X = Fe,Co,Ni) in the nonmagnetic state.

TABLE II. Calculated elastic constants (C_{ij}), bulk modulus (B_H), shear modulus (G_H), and Young's modulus (Y) in GPa as well as Debye temperature (Θ_D), Poisson's ratio (ν), and compressibility (β_H in GPa^{-1}) of ThXAsN (X = Fe,Co,Ni). For comparison, the mechanical properties of LaFeAsO (a parent compound of the 1111 Fe-based superconductor family) are also listed here.

	ThFeAsN	ThCoAsN	ThNiAsN	LaFeAsO[a]
C_{11}	211	211	235	192
C_{12}	74	64	76	56
C_{13}	68	72	85	62
C_{33}	105	109	120	145
C_{44}	95	57	74	44
C_{66}	39	44	56	78
B_H	99	101	114	99
G_H	61	51	60	57
Y	151	130	153	142
ν	0.24	0.28	0.27	0.25
β_H	0.0101	0.0099	0.0087	0.0102
Θ_D (K)	417	381	385	441

[a]Reference [44].

A. Elastic constants and mechanical stability

All calculated elastic constants are presented in Table II. They all are positive (see Table II) and obey the well-known Born criterion of mechanical stability [52]. Table II indicates that the C_{33} values of all three systems are well above the limit of the elastic stability, i.e., $C_{33} > C^* = 2C_{13}^2/(C_{11} + C_{12})$ [53]. For all three systems we have $B > G$, which indicates that the shear modulus G is the parameter that dictates the mechanical stability of the systems under consideration. Interestingly, Table II indicates that our calculated values of the elastic constants and elastic modulus are similar to the theoretical values of LaFeAsO [44]. Although LaFeAsO and ThFeAsN have a very similar lateral lattice constant (a = 4.035 Å for LaFeAsO [54]), the vertical lattice constant c of ThFeAsN is much smaller than that of LaFeAsO (c = 8.741 Å [54]). This pronounced difference in c would cause some internal uniaxial pressure in ThFeAsN along the c-axis. In spite of this pronounced structural difference, mechanical properties and elastic constants of these two compounds are very similar (Table II).

However, our calculated bulk modulus of ThFeAsN is lower than the bulk modulus estimated theoretically by Albedah *et al.* [33]. It turns out that the bulk modulus of these systems ($\sim$100 GPa) is smaller than that of other classes of high-T_c SCs such as MgB$_2$ ($\sim$122–161 GPa) [55] and YBa$_2$Cu$_3$O$_7$ ($\sim$200 GPa) [56]. Thus, in comparison to these high-T_c SCs, ThXAsN (X = Fe,Co,Ni) are relatively soft materials with high compressibilities. Young's modulus determines the stiffness of materials. Therefore, ThNiAsN has the highest and ThCoAsN has the lowest stiffness. A material is considered to be brittle if it satisfies the well-known Pough's criterion $B/G < 1.75$. Our results indicate that ThFeAsN lies in the boundary of brittle and plastic states as does that of the LaFeAsO compound. On the contrary, ThNiAsN and ThCoAsN systems clearly show plastic behavior. The values of Poisson's ratios indicate the ionic nature of bonding in these three compounds.

TABLE III. Ratio of the in-plane plasma frequency to the out-of-plane plasma frequency (ω_P^a/ω_P^c), c/a ratio, ratio of out-of-plane and in-plane Fe(Ni/Co)-Fe(Ni/Co) distances (d_{X-X}^c/d_{X-X}^a), and superconducting transition temperature (T_c) of some Fe-based SCs along with ThXAsN (X = Fe, Co, Ni).

System	ω_P^a/ω_P^c	c/a	d_{X-X}^c/d_{X-X}^a	Expt. $T_c^{\max}$ (K)
SrFeAsF[a]	19.892	2.2426	3.1715	56[b]
LaFeAsO[a]	8.9467	2.1656	3.0626	52[c]
FeSe[a]	4.1119	1.4656	2.0727	8[d]
LiFeAs[a]	3.2181	1.6785	2.3738	18[e]
BaFe$_2$As$_2$[a]	3.2926	3.285	2.3228	38[f]
ThFeAsN	3.0621	2.1069	2.9797	30[g]
ThCoAsN	6.3682	2.06	2.9144	
ThNiAsN	7.0934	1.957	2.7683	4.3[h]

[a]Reference [57].
[b]Reference [59] (doped compound).
[c]Reference [60] (doped compound).
[d]Reference [61].
[e]Reference [62].
[f]Reference [63] (doped compound).
[g]Reference [26].
[h]Reference [30].

B. Plasma frequency and effective dimensionality

Electronic structure calculations can provide important information about the effective dimensionality of a system through various quantities, such as dispersionless (flat) energy bands along certain symmetry lines, and van Hove singularities in density of states. A simple quantitative estimate of the effective dimensionality can be acquired by calculating plasma frequencies along the principal axes of a crystal [57]. The plasma frequency tensor $\omega_{P(\alpha\beta)}^2$ can be calculated from first principles as an integral over the Fermi surface using the relation [58]

$$\omega_{P(\alpha\beta)}^2 = -\frac{4\pi e^2}{V\hbar^2} \sum_{n,k} 2g_k \frac{\partial f(\epsilon_{nk})}{\partial \epsilon} \left(e_\alpha \frac{\partial \epsilon_{nk}}{\partial k}\right)\left(e_\beta \frac{\partial \epsilon_{nk}}{\partial k}\right),$$

where g_k is the weight factor of the **k** point, $f(\epsilon_{nk})$ is the Fermi-Dirac function, and e_α and e_β are the unit vectors in the α and β directions. respectively. V is the unit cell volume, e is the electron charge, $\hbar$ is the reduced Planck constant, and ϵ_{nk} are the energy eigenvalues.

Here we evaluate the plasma frequencies of all ThXAsN (X = Fe, Co, Ni) along the crystalline axes, and we compare our results with some other Fe-based SCs [57], including LaFeAsO, one of the parent compounds of the 1111 family. In Table III, we depict the calculated ratio of the in-plane plasma frequency ω_P^a to the out-of-plane plasma frequency ω_P^c. Also in Table III, we present some important structural parameters as well as superconducting transition temperature for these SCs.

It is evident from Table III that the plasma frequency ratio of ThFeAsN is significantly smaller than that of LaFeAsO. This implies that ThFeAsN is more 3D-like, which in turn make it the least anisotropic among all the compounds listed in Table III. Moreover, the values of c/a ratio as well as $d_{\text{Fe-Fe}}^c/d_{\text{Fe-Fe}}^a$ are also smaller than that of LaFeAsO. More
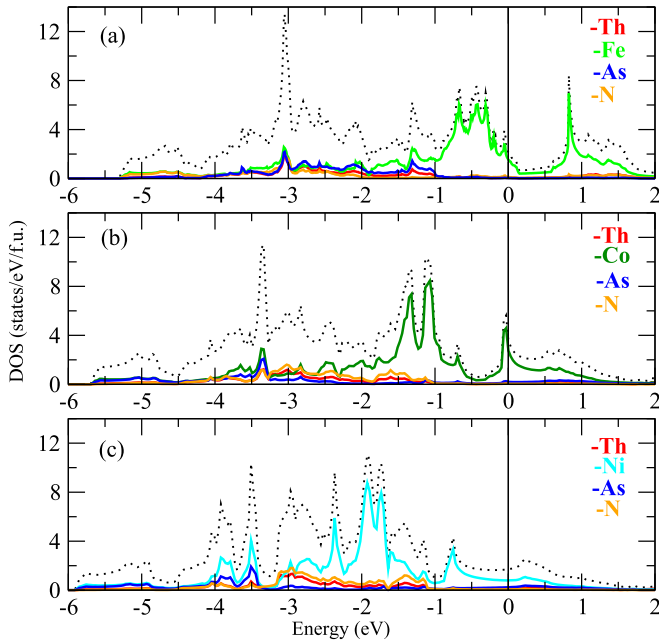
FIG. 2. Calculated total (dotted line) and atom-projected density of states of (a) ThFeAsN, (b) ThCoAsN, and (c) ThNiAsN. The Fermi energy is at 0 eV.

FIG. 3. Calculated transition metal d orbital-projected density of states (PDOS) of (a)–(d) ThFeAsN, (e)–(h) ThCoAsN, and (i)–(l) ThNiAsN.

3D-like electronic structure goes against the Fermi surface nesting, and this may be the reason for not having the SDW ordering, which was observed in LaFeAsO. On the other hand, the plasma frequency ratios in ThCoAsN and ThNiAsN are higher than that of ThFeAsN. This also indicates that ThCoAsN and ThNiAsN possess a more 2D-like electronic structure as compared to ThFeAsN. The ratio of the shortest interlayer to the shortest intralayer Fe(Ni/Co)-Fe(Ni/Co) distance is $c/\sqrt{2}a$ for the 122 systems and $\sqrt{2}c/a$ for the others, including the three systems studied here. However, ThFeAsN violates the general trend of proportionality of ω_P^a/ω_P^c to that of $d_{\text{Fe-Fe}}^c/d_{\text{Fe-Fe}}^a$ for the Fe-pnictide SCs.

C. Electronic structure

Low-energy electronic structure plays a key role in superconductivity. In this subsection, therefore, we present the calculated electronic structures of ThXAsN (X = Fe, Co, Ni). First, we display the total and atom-projected density of states (DOS) for ThFeAsN, ThCoAsN, and ThNiAsN in Fig. 2. We notice that overall, the DOS spectra for these three compounds are rather similar except that the Fermi levels (E_F) for the three compounds are located at the different positions. This may be expected since they are isostructural. In ThFeAsN, the DOS near E_F is dominated by transition metal (X) (Fe in this case) d-orbitals, which form two peaks, namely one broad peak just below E_F and one sharp peak located at ∼0.8 eV above E_F [see Fig. 2(a)]. There is a pseudogap between the two DOS peaks, and the Fermi level is located at the lower edge of the pseudogap. This gives rise to a moderate DOS at E_F of 2.3 states/eV/f.u. for ThFeAsN. As one moves from ThFeAsN to ThCoAsN, ThCoAsN has an additional valence electron and thus the Fermi level is raised to sit nearly right on the upper peak [see Fig. 2(b)]. This results in a large DOS
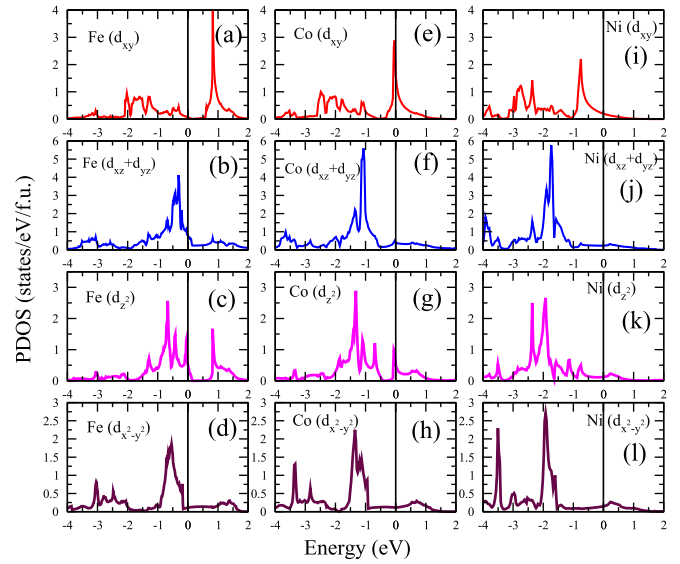
at E_F of 3.6 states/eV/f.u. for ThCoAsN. In ThCoAsN, therefore, a sharp peak in the DOS (mainly coming from Co atoms) at the Fermi level is observed. A large DOS at E_F may be important for superconductivity as it increases the possibility of electron-electron pairing. Unfortunately, a large DOS at E_F would also cause the Stoner instability [64,65], leading to the ferromagnetism in the Co system (see the next section). As one moves onto ThNiAsN, E_F is further raised to the rather flat upper part of the d-dominated band above the sharp peak [see Fig. 2(c)] because ThNiAsN has one more electron than ThCoAsN. Figure 2(c) shows that in this energy range, there are significant contributions from anion p orbitals, indicating a significant hybridization among the Ni d and anion p orbitals. This leads to the formation of rather dispersive bands across the Fermi level [see Fig. 4(c)], and thus results in the lowest DOS at E_F (1.7 states/eV/f.u.) for ThNiAsN among the three compounds. We notice that our calculated DOSs for ThFeAsN and ThNiAsN agree well with previous experiments as well as theoretical calculations [27,32,33,35].

In Fig. 3, we show the X d orbital-projected DOS of ThXAsN (X = Fe, Co, Ni). In the Fe system, d_{yz}, d_{xz}, and d_{z^2} orbitals dominate the DOS in the vicinity of the Fermi level, whereas in the Co system the DOS near E_F is mainly derived from the d_{xy} orbital. In fact, the sharp peak in the DOS for the Co d_{xy} orbital is observed at the Fermi level. Lastly in the Ni system, no particular dominance of any particular orbital is observed. Overall, ThFeAsN and ThCoAsN show more multiorbital characteristics near E_F than that of ThNiAsN. Pseudo-gap-like regions in the DOS of ThFeAsN and ThCoAsN are mainly due to the d_{z^2} orbital, which is extended along the c-axis.

Next we present the calculated band structures of ThXAsN (X = Fe, Co, Ni) in Fig. 4. We also display the orbital-projected band structures of ThFeAsN, ThCoAsN, and ThNiAsN in Figs. 5, 6, and 7, respectively. Electronic band dispersions near the Fermi level for the Fe, Co, and Ni systems
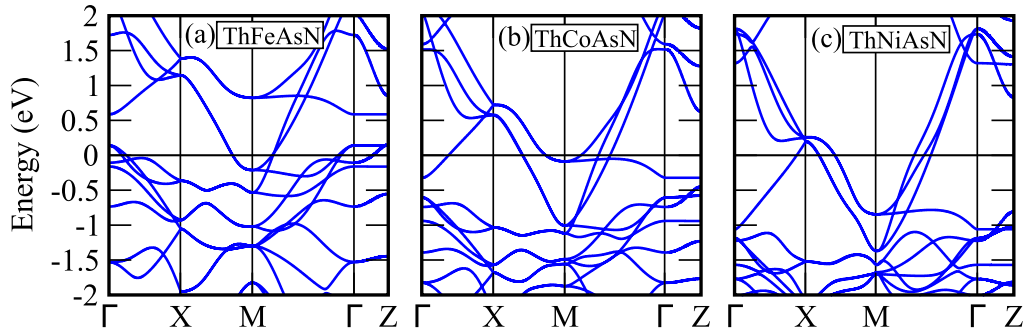
FIG. 4. Calculated band structures of (a) ThFeAsN, (b) ThCoAsN, and (c) ThNiAsN.

are quite different from each other. In particular, the band structure of ThFeAsN is significantly different from the other two systems. The band structure of ThFeAsN is quite similar to that of F-doped LaFeAsO [66]. Interestingly, the band structure of ThCoAsN possesses a Co d_{xy} orbital dominated flat band just below E_F along the high-symmetry Γ-M line [see Figs. 4(b) and 6]. Orbital characters of the bands near E_F are also different for all three systems. In ThFeAsN, a rather flat band near E_F coming from the Fe d_{z^2} orbital is observed around the Γ point (Fig. 5). On the other hand, this particular feature is missing in the band structure of ThNi-AsN. Flat bands indicate a large number of electronic states. Therefore, the presence of flat bands near E_F would enhance the possibility of electron pairing (formation of Cooper pairs), irrespective of the superconducting pairing mechanism.

Calculated Fermi surfaces (FSs) of the ThXAsN compounds are depicted in Fig. 8. For the Fe system, the FS consists of three FS pockets [panels 1–3 in Fig. 8(a)] at the Γ point and two-electron FS sheets [panels 4 and 5 in Fig. 8(a)] at the M ($\pi, \pi, 0$) point in the Brillouin zone. This Fermi surface topology of ThFeAsN is quite similar to that of other Fe-based SCs such as LaFeAsO [67,68]. One of the three-hole FS pockets (panel 2) at the Γ point is nearly two-dimensional and thus looks like a circular cylinder, whereas the two-electron FS sheets (panels 4 and 5) at the zone corners

(the M points) are more 3D-like. For the Co and Ni systems, in contrast, there are three-electron FS sheets (panels 2–4) around the M point and a one-hole FS (panel 1) at the X point. There is no FS sheet at the Γ point in these two systems. Since the appearance of FSs is at different points for ThFeAsN and ThCo(Ni)AsN, interband nesting vectors are different for these systems. These significant differences may affect the intraband and interband nesting properties of these systems, which could play a role in the possible formation of spin and charge density waves as well as superconductivity in this type of SC. The absence of hole FS pockets at the center of the Brillouin zone in ThCoAsN and ThNiAsN does not help interband FS nesting, and hence these two systems are not likely to show FS nesting-driven spin/charge density wave ordering.

We also perform a Bader analysis [69] on the charge densities in ThXAsN ($X =$ Fe, Co, Ni), and the results are listed in Table IV. In ThFeAsN, a loss of 0.38 electrons in the [FeAs]$^-$ layer is observed (see Table IV), which is consistent with the previous theoretical study [32]. In ThCoAsN and ThNiAsN, we find a loss of 0.51 and 0.40 electrons in the [Co/NiAs]$^-$ layer, respectively. In ThCoAsN, the interlayer charge transfer is larger as compared to the other two systems. More charge transfer between the adjacent layers indicates the enhancement of the ionic character in the interlayer bonding.
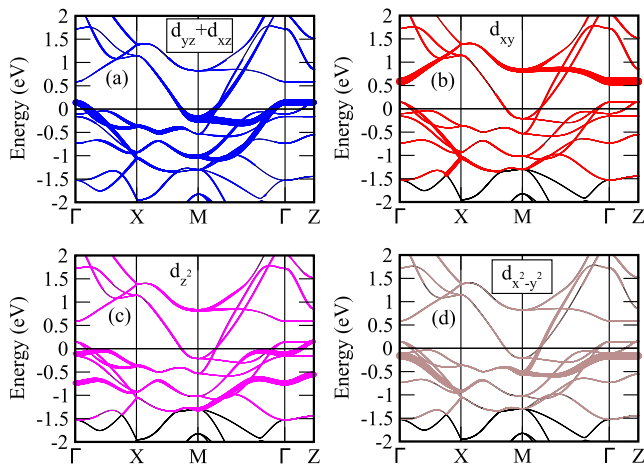

FIG. 5. Calculated Fe (a) $d_{yz} + d_{xz}$ (blue), (b) d_{xy} (red), (c) d_{z^2} (magenta), and (d) $d_{x^2-y^2}$ (brown) orbital-projected band structures of ThFeAsN.
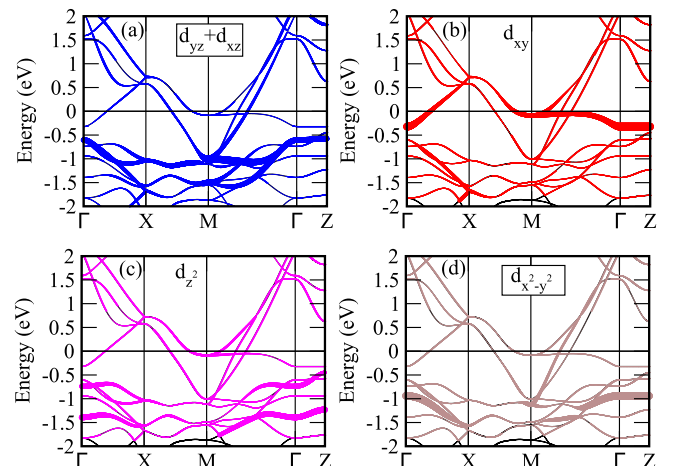

FIG. 6. Calculated Co (a) $d_{yz} + d_{xz}$ (blue), (b) d_{xy} (red), (c) d_{z^2} (magenta), and (d) $d_{x^2-y^2}$ (brown) orbital-projected band structures of ThCoAsN.
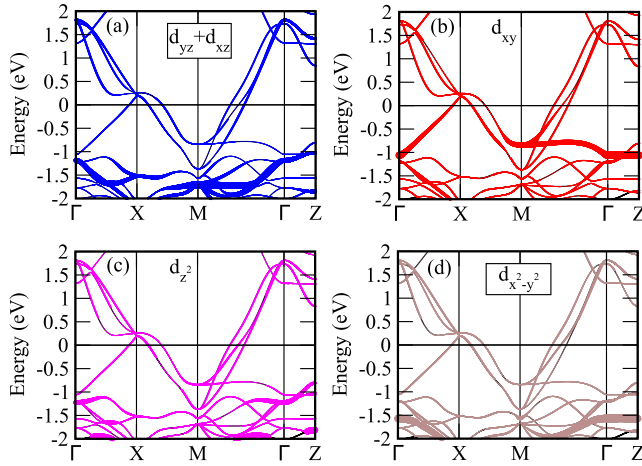
FIG. 7. Calculated Ni (a) $d_{yz} + d_{xz}$ (blue), (b) d_{xy} (red), (c) d_{z^2} (magenta), and (d) $d_{x^2-y^2}$ (brown) orbital-projected band structures of ThNiAsN.

As a result, the interlayer bonds that are responsible for the common stability of the crystal are weakest in ThFeAsN and strongest for ThCoAsN. Thus, ThFeAsN is softer than ThCoAsN, and the softness of ThNiAsN lies between them.

D. Phonon dispersion and electron-phonon coupling

Now let us examine the calculated lattice-dynamical properties of ThXAsN (X = Fe, Co, Ni). In Figs. 9(a), 10(a), and 11(a), we present the calculated phonon dispersion relations of ThFeAsN, ThCoAsN, and ThNiAsN, respectively. Since all three systems have eight atoms per unit cell, there are 24 branches with three acoustic and 21 optical phonon branches. First of all, it is clear from these phonon dispersion relations that there are no imaginary frequencies, thus indicating that these systems are dynamically stable. Second, there exists a clear gap in the phonon dispersion relations in all the three systems (see Figs. 9, 10, and 11). Interestingly, the gap in the Fe system is smaller than that of the Co and Ni systems. This difference is due to the differences in the atomic mass
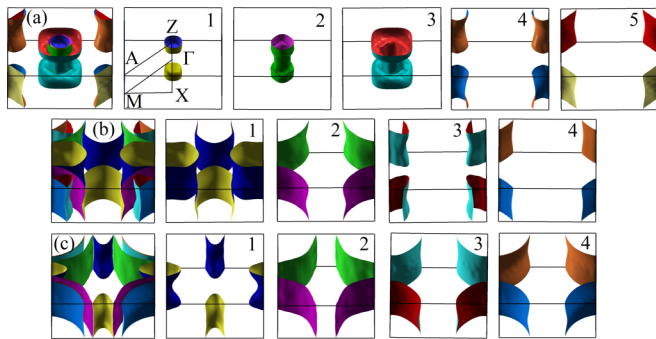

FIG. 8. Calculated Fermi surface (FS) of (a) ThFeAsN, (b) ThCoAsN, and (c) ThNiAsN. In ThFeAsN, there are three hole FSs (panels 1–3) at the Γ point and two electron FSs (panels 4 and 5) at the M point. In ThCoAsN and ThNiAsN, there are one-hole FS (panel 1) at the X point and three-electron FSs (panels 2–4) at the M point.

TABLE IV. Calculated electronic charges by the Bader analysis, and also ideal ionic charges for the atomic species in ThXAsN (X = Fe, Co, Ni).

Species	Bader analysis	Purely ionic
	(a) ThFeAsN	
Th	9.77	8 (Th^{4+})
Fe	7.88	6 (Fe^{2+})
As	5.73	8 (As^{3-})
N	6.61	8 (N^{3-})
ThN	16.38	16 (ThN$^+$)
FeAs	13.61	14 (FeAs$^-$)
	(b) ThCoAsN	
Th	10.22	8 (Th^{4+})
Co	8.99	7 (Co^{2+})
As	5.49	8 (As^{3-})
N	6.29	8 (N^{3-})
ThN	16.51	16 (ThN$^+$)
CoAs	14.48	15 (CoAs$^-$)
	(c) ThNiAsN	
Th	9.81	8 (Th^{4+})
Ni	10.04	8 (Ni^{2+})
As	5.56	8 (As^{3-})
N	6.59	8 (N^{3-})
ThN	16.40	16 (ThN$^+$)
NiAs	15.60	16 (NiAs$^-$)

among the Fe, Co, and Ni atoms. The six high-lying optical branches above the gap are mainly due to the lighter N and As atoms, thus being almost the same in all three systems. On the other hand, the 18 lower frequency branches including three
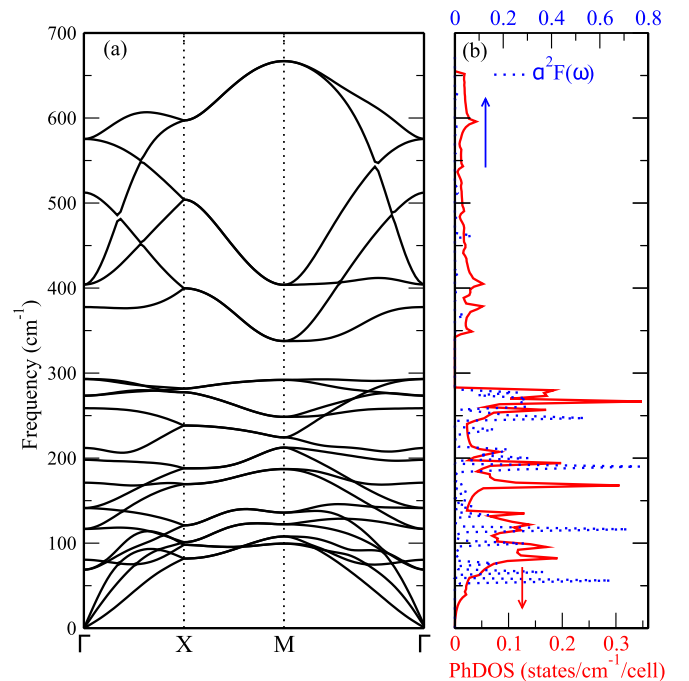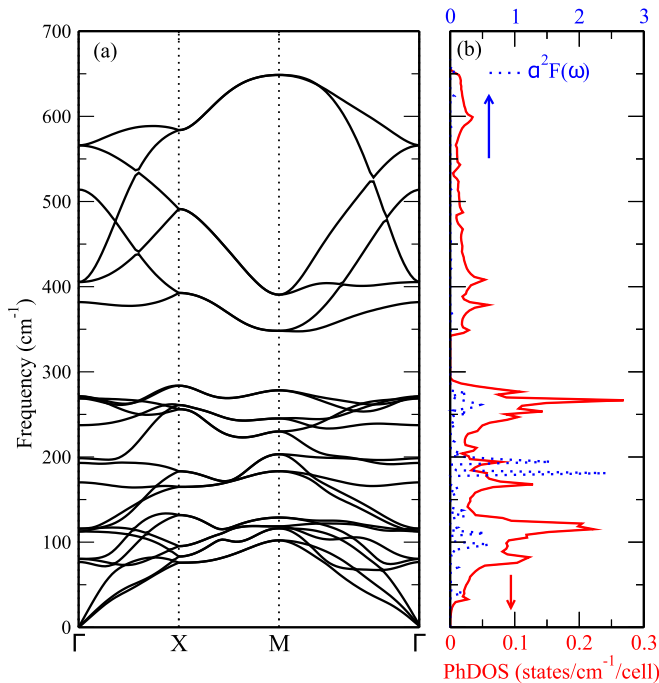

FIG. 9. (a) Phonon dispersion relations, (b) Eliashberg spectral function [$\alpha^2 F(\omega)$] (blue dotted line) and phonon density of states (PhDOS) (red line) of ThFeAsN.

FIG. 10. (a) Phonon dispersion relations, (b) Eliashberg spectral function $[\alpha^2 F(\omega)]$ (blue dotted line) and phonon density of states (PhDOS) (red line) of ThCoAsN.

acoustic modes below the gap come predominantly from the Th and transition-metal atoms. Consequently, the bandwidth of these lower frequency branches become narrower as Fe is replaced by heavier Co and Ni, and this gives rise to a slightly larger gap in ThCoAsN (Fig. 10) and ThNiAsN (Fig. 11)
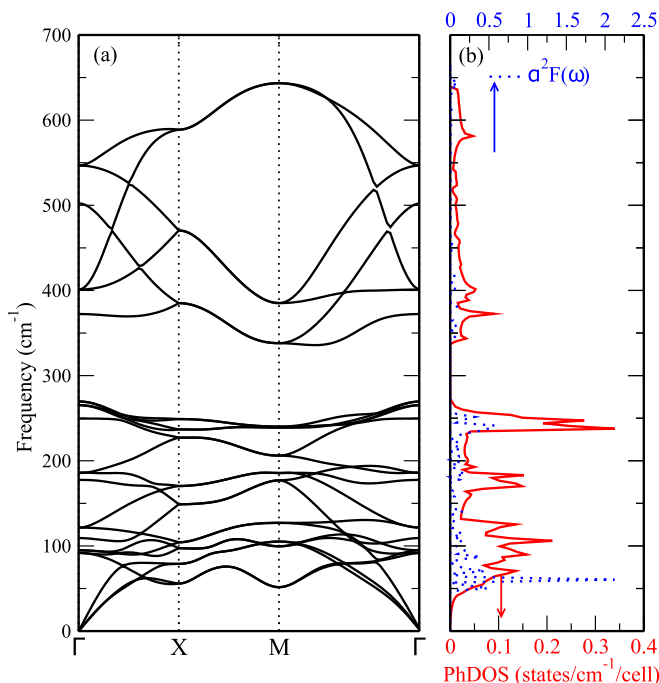

FIG. 11. (a) Phonon dispersion relations, (b) Eliashberg spectral function $[\alpha^2 F(\omega)]$ (blue dotted line) and phonon density of states (PhDOS) (red line) of ThNiAsN.

TABLE V. Calculated electron-phonon coupling constant (λ), logarithmic average phonon frequency ($\omega_{\log}$), and superconducting transition temperature T_c of ThXAsN. Experimental T_c values are also listed in parentheses.

System	λ	$\omega_{\log}$ (K)	$N(E_F)$ (states/eV/f.u.)	T_c (K) Theory (Expt.)
ThFeAsN	0.28	199	2.01	0.05 (30[a])
ThCoAsN	0.65	221	4.22	6.4
ThNiAsN	0.64	120	1.81	3.4 (4.3[b])

[a]Reference [26].
[b]Reference [30].

than in ThFeAsN (Fig. 9). We notice that phonon dispersion relations of ThFeAsN are quite different from that of LaFeAsO [54]. In particular, there is no such gap as mentioned above in LaFeAsO [54]. We also notice that although the lattice-dynamical properties of ThNiAsN have already been studied theoretically within the DFPT [31], no study on lattice dynamics of ThFeAsN and ThCoAsN has been reported. The present phonon dispersion of ThNiAsN agrees rather well with that reported in [31].

In Figs. 9(b), 10(b), and 11(b), we display the calculated phonon density of states (phDOS) as well as Eliashberg spectral functions $[\alpha^2 F(\omega)]$ of ThFeAsN, ThCoAsN, and ThNiAsN, respectively. We notice that the phDOS in the low-frequency manifold is many times larger than the high-lying optical branches above the gap, because there are many narrow branches in the manifold. The $\alpha^2 F(\omega)$ spectral functions, which reflect the electron-phonon coupling strength, roughly follow the phDOS spectra [see Figs. 9(b), 10(b), and 11(b)], i.e., we can regard an $\alpha^2 F(\omega)$ spectral function as the corresponding phDOS spectrum modified by the electron-phonon coupling matrix elements. As a result, the Eliashberg function $\alpha^2 F(\omega)$ is dominated by the contribution from the phonon bands in the low-frequency manifold for all three compounds. By integrating $\alpha^2 F(\omega)/\omega$ over the entire frequency range [see Eq. (2)], one can obtain the electron-phonon coupling constant (λ). It is evident from Figs. 9(b), 10(b), and 11(b) that the magnitude of the $\alpha^2 F(\omega)$ spectrum is highest in the Co system and lowest in the Fe system. Therefore, we find a lowest λ value for the Fe system and a highest λ value for the Co system (see Table V). Nevertheless, the calculated λ value (0.64) for the Ni system is only very slightly smaller than the Co system (0.65).

Finally, given the λ value as well as other phonon and electron parameters, we can use the Allen-Dynes-modified McMillan formula [Eq. (4)] to estimate the superconducting transition temperature (T_c). Here we treat the screened electron-electron repulsion μ as an empirical parameter and set $\mu = 0.10$ [31]. Our calculated T_c values for all the compounds are listed in Table V, together with the available experimental T_c values. We notice that our calculated T_c of 3.4 K for ThNiAsN agrees very well with the previous calculation (3.5 K) [31] and also with the experimental T_c of 4.3 K [30]. However, our calculated $T_c = 0.05$ K for ThFeAsN is orders of magnitude smaller than the observed T_c (over 30 K) [26]. This is because the calculated electron-phonon coupling strength λ (0.28) for ThFeAsN is much smaller than ThNiAsN

(0.64). Clearly, this indicates that electron-phonon coupling cannot be the primary mechanism of the high-T_c superconductivity observed in ThFeAsN. Interestingly, ThCoAsN is predicted to have the highest T_c of 6.4 K (Table V). We notice that although the calculated λ values for ThCoAsN and ThNiAsN are nearly equal, the calculated T_c of ThCoAsN is significantly higher than ThNiAsN. This could be attributed to the fact that the averaged logarithmic phonon frequency $\omega_{\log}$ of ThCoAsN is nearly twice as large as ThNiAsN [see Table V and Eq. (4)].

IV. DISCUSSION

In this section, we first study the possible magnetic states in these compounds and the effect of their presence on the band structures. As reported in the preceding section, our DFPT calculations predict a T_c value for ThFeAsN that is much too small compared with the observed value (see Table V). Therefore, also in this section, we discuss the effect of possible SDW-type AF orders on the electron-phonon coupling and superconductivity in ThFeAsN. We then examine the effect of anion As height on the electronic structure, especially the Fermi surface of nonmagnetic ThFeAsN.

A. Magnetism

Here we consider three possible magnetic structures in ThXAsN ($X =$ Fe, Co, Ni), i.e., the ferromagnetic (FM) as well as the checkerboard antiferromagnetic (c-AF) and stripe antiferromagnetic (s-AF) structures [32]. The magnetic unit cell of the FM and c-AF structures is the same as the chemical unit cell, while the magnetic unit cell for the s-AF structure is $\sqrt{2}a \times \sqrt{2}a \times c$ with the Cartesian coordinates rotated 45°. Using the lattice constants listed in Table I, we perform structural optimization calculations for these FM and AF states for all three compounds with the atomic positions fully relaxed, as described in Sec. II. The calculated properties of the magnetic as well as nonmagnetic ThXAsN ($X =$ Fe, Co, Ni) are listed in Table VI. First of all, we find that in ThFeAsN, both c-AF and s-AF states could be stabilized with the s-AF state having the lowest total energy (Table VI), while the FM state cannot be stabilized. This is consistent with previous theoretical calculations [32,35]. Nonetheless, as mentioned in Sec. I, no long-range magnetic order has been experimentally observed in ThFeAsN [26]. This suggests that the GGA calculations may overestimate the tendency toward the antiferromagnetism in ThFeAsN. Interestingly, Table VI shows that the anion height h_{As} in the s-AF phase (1.26 Å) is significantly larger than that in the NM case (1.18 Å) and thus moves closer to the experimental value of 1.30 Å [40]. Second, our calculations indicate that ThCoAsN is ferromagnetic, and no AF states can be stabilized. Table VI shows that the calculated Fe and Co magnetic moments are significant, although they are considerably smaller than the Fe and Co magnetic moments in ferromagnetic Fe and Co metals, respectively. The calculated Th, As, and N magnetic moments are smaller than $0.01\mu_B$ and are thus not listed in Table VI. Finally, we find that no magnetic state can be stabilized in ThNiAsN, i.e., ThNiAsN is nonmagnetic.

TABLE VI. Total energy [ΔE in meV/f.u., relative to the nonmagnetic state (NM)], density of states at the Fermi level [$N(E_F)$ in states/eV/spin/f.u.], total magnetic moment (m_s^{tot} in μ_B/f.u.), magnetic moments on transition-metal atoms (m_s^{Fe}, m_s^{Co} in μ_B), the As height (h_{As} in Å), As (z_{As}), and Th (z_{Th}) positions in ThFeAsN, ThCoAsN, and ThNiAsN in the NM, ferromagnetic (FM), checkerboard antiferromagnetic (c-AF), and stripe antiferromagnetic (s-AF) states. Calculated magnetic moments on non-transition-metal atoms are less than $0.01\mu_B$ and thus are not listed here. Note that the FM and AF states cannot be stabilized in ThFeAsN and ThCoAsN, respectively. Moreover, no FM nor AF states can be stabilized in ThNiAsN.

| | ThFeAsN | | | ThCoAsN | | ThNiAsN |
	NM	c-AF	s-AF	NM	FM	NM
ΔE	0	-14.12	-82.79	0	-34.28	0
$N(E_F)$	2.29	1.87	0.19	3.6	0.88 (up)	1.70
					0.43 (dn)	
$m_s^{Fe/Co}$	0	1.37	1.89	0	0.58	0
m_s^{tot}	0	0		0	1.16	0
z_{As}	0.6388	0.6430	0.6483	0.6404	0.6405	0.6405
z_{Th}	0.1382	0.1377	0.1374	0.1377	0.1396	0.1396
h_{As}	1.18	1.22	1.26	1.17	1.17	1.12

The DOS spectra and band structures of the c-AF and s-AF ThFeAsN and FM ThCoAsN are plotted in Figs. 12, 13, and 14, respectively. Roughly speaking, the DOS spectra of NM, c-AF, and s-AF ThFeAsN are rather similar [see Figs. 2(a), 12(a), and 13(a)]. In particular, there is a valley near E_F. One significant difference is that the E_F sits on the lower slope of the valley in NM ThFeAsN, while it is located at the bottom of the valley in the c-AF and s-AF cases. This results in a much smaller DOS at E_F in s-AF ThFeAsN (0.19 states/eV/f.u.) compared with NM ThFeAsN (Table VI). Overall, the band structures of c-AF and s-AF ThFeAsN are also quite similar, except that the number of energy bands in s-AF ThFeAsN is twice as many as in c-AF because the number of atoms in the s-AF ThFeAsN unit cell is doubled. Nonetheless, the energy bands in the vicinity of E_F in NM, c-AF, and s-AF ThFeAsN are all quite different. Figure 14(b) shows that in FM ThCoAsN, the energy bands are significantly spin-split with spin-down bands (blue curves) moved upward and spin-up bands (red curves) shifted downward. Consequently, there is no flat band near E_F, and the DOS spectrum near E_F in FM ThCoAsN [Fig. 14(a)] differs significantly from that of NM ThCoAsN [Fig. 2(b)]. In particular, the DOS at the Fermi
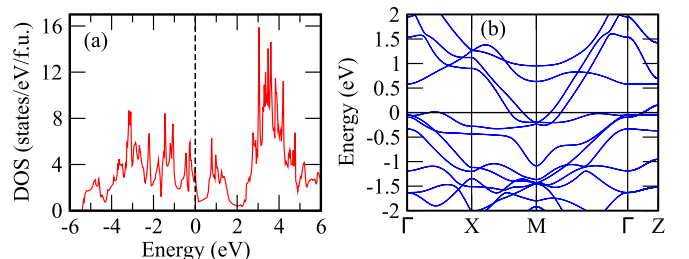

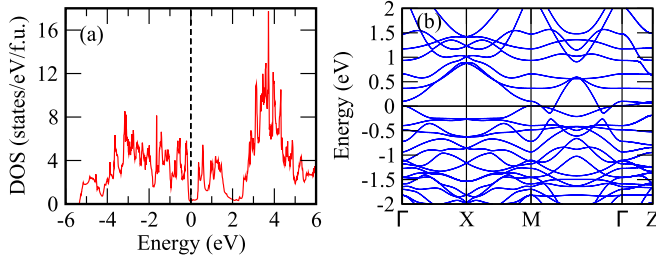FIG. 12. Calculated (a) density of states and (b) band structure of checkerboard antiferromagnetic (c-AF) ThFeAsN.

FIG. 13. Calculated (a) density of states and (b) band structure of stripe antiferromagnetic (s-AF) ThFeAsN.

level in FM ThCoAsN gets much reduced compared with NM ThCoAsN (see Table VI).

Since there is theoretical evidence for the AF orders in ThFeAsN, especially the SDW-type s-AF order (Table VI), we want to discuss the possible effects of the SDW-type AF order on the electron-phonon coupling constant and hence superconductivity in ThFeAsN. It was recently observed that the electron-phonon coupling in some Fe-based SCs increases in the presence of the AF order [20]. It was also shown that the electron-phonon coupling constant could be further increased when the soft out-of-plane lattice vibrations were taken into account [18]. For a collinear AF system, occupied up and down spin electron orbitals are located on a different subset of magnetic atoms in the unit cell. On the other hand, in the NM state, orbitals of both spin types exist at equal amplitudes on both Fe atoms in the unit cell. When the atoms vibrate around their equilibrium positions, the effective potential is changed accordingly, which leads to an enhancement of the electron-phonon coupling matrix elements, so that the electron-phonon coupling becomes doubled at the occupied position for this particular spin orientation [18]. According to Ref. [34], one can write the effective electron-phonon coupling on the Fermi surface as

$$\lambda_{\text{eff}} = \lambda_{E_F} R_{\text{ph}}^2 R_{\text{SDW}}^2 R_g^2, \tag{5}$$

where R_{ph} is the amplification factor due to the soft out-of-plane lattice vibrations, and it turns out to be 2 in the AF background [20]. R_{SDW} is the amplification factor due to the AF order, which is also 2 [18]. R_g is the amplification due to the electrons scattered below the Fermi surface, which we ignore in the present calculation. In the strong-coupling case, the renormalized effective electron-phonon coupling can be written as [34] $\lambda_{\text{eff}}^* = \lambda_{\text{eff}}/(\lambda_{\text{eff}} + 1)$ and the renormalized screened electron-electron repulsion can be written as $\mu_{\text{eff}}^* =$
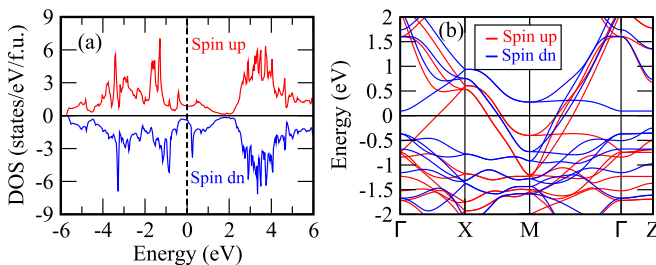

FIG. 14. Calculated spin-polarized (a) density of states and (b) band structure of ferromagnetic ThCoAsN.
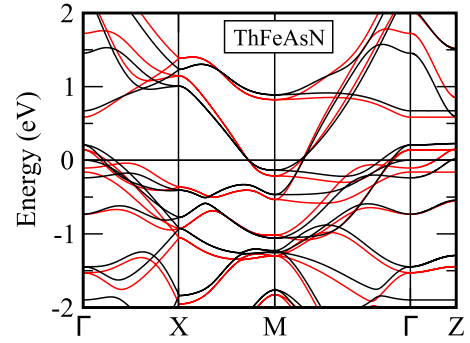

FIG. 15. Band structures of nonmagnetic ThFeAsN calculated using experimental (black lines) and theoretical (red) atomic positions.

$\mu_{\text{eff}}/(\mu_{\text{eff}} + 1)$. After employing all the amplification factors in λ, we get an effective electron-phonon coupling constant λ_{eff} of 0.82 for ThFeAsN. This value of λ_{eff} together with the renormalized μ would result in a T_c of 10.4 K, being in the same order of magnitude as the experimental T_c value of 30 K. This indicates that an accurate treatment of the combined effect of the electron-phonon coupling and antiferromagnetism in ThFeAsN would be fruitful, which, however, is a project for the future.

B. Anion As height and electronic structure

In this subsection, we examine the effect of the anion height (i.e., the As atomic position relative to the Fe-Fe plane h_{As}) on the electronic structure of ThFeAsN. We plot the band structure and Fermi surface of ThFeAsN, respectively, in Figs. 15 and 16, calculated using both the theoretical and experimental ($z_{\text{As}} = 0.6522$, $z_{\text{Th}} = 0.1380$) [40] atomic positions with the fixed experimental lattice constants (see Table I). Figure 15 show that low-energy band structures of ThFeAsN calculated using the theoretical and experimental atomic positions differ significantly. In particular, the number of bands that cross the Fermi level in the vicinity of the Γ point is different. This results in the different FS shapes and different numbers of the FS pockets for the two cases (Fig. 16). One pronounced difference is that the FS sheets centered at the Γ point calculated using the experimental atomic positions are much more two-dimensional than that obtained using the theoretical atomic positions (see Fig. 16). This would affect the degree of the FS nesting in ThFeAsN. The FS nesting is believed to play a crucial role in the appearance of various exotic phases including superconductivity in the Fe-based
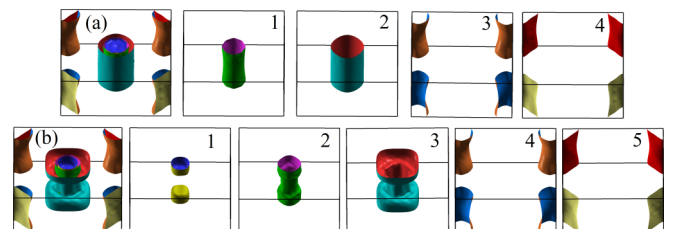

FIG. 16. Fermi surfaces of nonmagnetic ThFeAsN calculated using (a) experimental and (b) theoretical atomic positions.

SCs [67,70]. These pronounced differences in the electronic structure of ThFeAsN are due to the significant difference in the anion height, which is caused by the GGA underestimation of the anion height [32,35]. Furthermore, our recent calculations [71] using the semilocal DFT-D3 exchange-correlation potential of Grimme and co-workers [72] to take into account the van der Waals interaction gave rise to an anion height that is identical to the GGA value. Therefore, we speculate that to theoretically obtain the accurate anion height in ThFeAsN, one should include the effect of magnetic fluctuation, which may play a major role in the physical properties including superconductivity in ThFeAsN.

V. CONCLUSIONS

Summarizing, we have carried out a comparative first-principles study of mechanical properties, electronic structure, phonon dispersion relations, electron-phonon coupling, and magnetism in isostructural superconductors ThFeAsN, ThCoAsN, and ThNiAsN. First, our calculated elastic constants indicate that all three compounds are mechanically stable. Our calculations also reveal that ThFeAsN lies in the boundary of brittle and plastic behavior, being similar to that of the LaFeAsO system. On the other hand, the Co and Ni systems show rather plastic behavior. The calculated plasma frequencies indicate that ThFeAsN possesses a more 3D-like electronic structure than that of the Co and Ni systems. Secondly, our calculated electronic structures indicate that overall, the three compounds have a rather similar electronic structure. Nonetheless, because of their different numbers of conduction electrons, their Fermi levels are located at rather different energy positions (see Fig. 2). This results in quite different low-energy band structures in the vicinity of the Fermi level (see Fig. 4). For example, the density of states at the Fermi level $N(E_F)$ for the Co system is twice as large as that for the Fe and Ni systems (see Table V). Topologies of the Fermi surface of the Ni and Co systems are quite similar, whereas the FS topology of the Fe system is very similar to that of the LaFeAsO system. The FS of ThFeAsN is mostly derived from Fe d_{z^2} and d_{xz+yz} orbitals, whereas for the Co system, it is dominated by the d_{xy} orbital. Thirdly, our calculated phonon dispersions show that these three systems are dynamically stable. Our electron-phonon coupling calculations indicate that ThCoAsN and ThNiAsN have nearly the same values of electron-phonon coupling constant λ while the λ value of ThFeAsN is less than half of that for the Co and Ni systems (Table V). As a result, ThCoAsN has the

highest superconducting transition temperature T_c of 6.4 K (Table V). The T_c for ThNiAsN is 3.4 K, which is quite close to the experimental value of 4.3 K. This indicates that the superconductivity in ThNiAsN is phonon-mediated. However, ThFeAsN has a nearly zero T_c of 0.05 K, which is far too small compared with the experimental value of $\sim$30 K (Table V).

In addition to the systematic calculations for NM ThXAsN (X = Fe, Co, Ni) mentioned above, we have also studied the effect of anion As height on the low-energy electronic structure of NM ThFeAsN and possible magnetic states in all three compounds. Interestingly, we find that the c-AF and s-AF structures can appear in ThFeAsN, although the FM state cannot be stabilized. Furthermore, the calculated anion height h_{As} in the s-AF state is much closer to the experimental value than in the NM state (Table VI). However, no long-range AF order has been observed. This suggests that the GGA calculations may overestimate the tendency toward the antiferromagnetism in ThFeAsN. Since there is theoretical evidence for the s-AF order in ThFeAsN (Table VI), we examine the possible effects of the SDW-type AF order on the electron-phonon coupling and hence superconductivity in ThFeAsN. We find a significant enhancement of λ when the SDW-type AF background and soft out-of-plane lattice vibrations are taken into consideration. This leads to a T_c of $\sim$10 K. We thus speculate that the superconductivity in ThFeAsN may be caused by mechanisms other than purely electron-phonon coupling, such as the SDW-type AF fluctuation-mediated one. Finally, ThCoAsN is predicted to be ferromagnetic while ThNiAsN is found to be nonmagnetic. If the ferromagnetism does occur in ThCoAsN, the superconductivity in NM ThCoAsN predicted in Sec. III will be suppressed due to the ferromagnetic pair breaking [73]. However, as mentioned above, the GGA calculations may overestimate the tendency toward the magnetism. Consequently, the predicted ferromagnetic state may not appear in ThCoAsN and hence the predicted superconductivity may be observed instead.

[1] Y. Kamihara, T. Watanabe, M. Hirano, and H. Hosono, J. Am. Chem. Soc. **130**, 3296 (2008).

[2] G. R. Stewart, Rev. Mod. Phys. **83**, 1589 (2011).

[3] N. Katayama, K. Kudo, S. Onari, T. Mizukami, K. Sugawara, Y. Sugiyama, Y. Kitahama, K. Iba, K. Fujimura, N. Nishimoto, M. Nohara, and H. Sawa, J. Phys. Soc. Jpn. **82**, 123702 (2013).

[4] A. Iyo, K. Kawashima, T. Kinjo, T. Nishio, S. Ishida, H. Fujihisa, Y. Gotoh, K. Kihou, H. Eisaki, and Y. Yoshida, J. Am. Chem. Soc. **138**, 3410 (2016).

[5] T. Watanabe, H. Yanagi, T. Kamiya, Y. Kamihara, H. Hiramatsu, M. Hirano, and H. Hosono, Inorg. Chem. **46**, 7719 (2007).

[6] T. Watanabe, H. Yanagi, Y. Kamihara, T. Kamiya, M. Hirano, and H. Hosono, J. Solid State Chem. **181**, 2117 (2008).

[7] F. Ronning, N. Kurita, E. D. Bauer, B. L. Scott, T. Park, T. Klimczuk, R. Movshovich, and J. D. Thompson, J. Phys.: Condens. Matter **20**, 342203 (2008).

[8] Y. Tomioka, S. Ishida, M. Nakajima, T. Ito, H. Kito, A. Iyo, H. Eisaki, and S. Uchida, Phys. Rev. B **79**, 132506 (2009).

[9] A. S. Sefat, A. Huq, M. A. McGuire, R. Jin, B. C. Sales, D. Mandrus, L. M. D. Cranswick, P. W. Stephens, and K. H. Stone, Phys. Rev. B **78**, 104505 (2008).

[10] A. S. Sefat, D. J. Singh, R. Jin, M. A. McGuire, B. C. Sales, F. Ronning, and D. Mandrus, Physica C **469**, 350 (2009).

[11] J. Dong, H. J. Zhang, G. Xu, Z. Li, G. Li, W. Z. Hu, D. Wu, G. F. Chen, X. Dai, J. L. Luo, Z. Fang, and N. L. Wang, Europhys. Lett. **83**, 27006 (2008).

[12] V. Cvetkovic and Z. Tesanovic, Europhys. Lett. **85**, 37002 (2009).

[13] V. Cvetkovic and Z. Tesanovic, Phys. Rev. B **80**, 024512 (2009).

[14] R. M. Fernandes, A. V. Chubukov, and J. Schmalian, Nat. Phys. **10**, 97 (2014).

[15] R. M. Fernandes, L. H. Van Bebber, S. Bhattacharya, P. Chandra, V. Keppens, D. Mandrus, M. A. McGuire, B. C. Sales, A. D. Sefat, and J. Schmalian, Phys. Rev. Lett. **105**, 157003 (2010).

[16] A. Subedi, D. J. Singh, and M.-H. Du, Phys. Rev. B **78**, 060506(R) (2008).

[17] A. Subedi and D. J. Singh, Phys. Rev. B **78**, 132511 (2008)

[18] S. Coh, M. L. Cohen, and S. G. Louie, Phys. Rev. B **94**, 104505 (2016).

[19] B. Li, Z. W. Xing, G. Q. Huang, and M. Liu, J. App. Phys. **111**, 033922 (2012).

[20] S. Deng, J. Köhler, and A. Simon, Phys. Rev. B **80**, 214508 (2009).

[21] I. I. Mazin, D. J. Singh, M. D. Johannes, and M. H. Du, Phys. Rev. Lett. **101**, 057003 (2008).

[22] K. Kuroki, S. Onari, R. Arita, H. Usui, Y. Tanaka, H. Kontani, and H. Aoki, Phys. Rev. Lett. **101**, 087004 (2008).

[23] A. V. Chubukov, D. V. Efremov, and I. Eremin, Phys. Rev. B **78**, 134512 (2008).

[24] P. J. Hirschfeld, M. M. Korshunov, and I. I. Mazin, Rep. Prog. Phys. **74**, 124508 (2011).

[25] I. Pallecchi, M. Eisterer, A. Malagoli, and M. Putti, Supercond. Sci. Technol. **28**, 114005 (2015).

[26] C. Wang, Z.-C. Wang, Y.-X. Mei, Y.-K. Li, L. Li, Z.-T. Tang, Y. Liu, P. Zhang, H.-F. Zhai, Z.-A. Xu, and G.-H. Cao, J. Am. Chem. Soc. **138**, 2170 (2016).

[27] T. Shiroka, T. Shang, C. Wang, G.-H. Cao, I. Eremin, H.-R. Ott, and J. Mesot, Nat. Commun. **8**, 156 (2017).

[28] I. Errea, M. Calandra, C. J. Pickard, J. Nelson, R. J. Needs, Y. Li, H. Liu, Y. Zhang, Y. Ma, and F. Mauri, Phys. Rev. Lett. **114**, 157004 (2015).

[29] Y. Li, J. Hao, H. Liu, Y. Li, and Y. Ma, J. Chem. Phys. **140**, 174712 (2014).

[30] Z.-C. Wang, Y.-T. Shao, C. Wang, Z. Wang, Z.-A. Xu, and G.-H. Cao, Europhys. Lett. **118**, 57004 (2017).

[31] Y. Yang, S.-Q. Feng, H.-Y. Lu, L.-T. Gu, and Z.-P. Chen, J. Supercond. Nov. Magn. **31**, 3153 (2018).

[32] G. Wang and X. Shi, Europhys. Lett. **113**, 67006 (2016)

[33] M. A. Albedah, F. Nejadsattari, Z. M. Stadnik, Z.-C. Wang, C. Wang, and G.-H. Cao, J. Alloys Compd. **695**, 1128 (2017).

[34] C. H. Wong and R. Lortz, arXiv:1902.06463v2.

[35] D. J. Singh, J. Alloys Compd. **687**, 786 (2016).

[36] J. P. Perdew, K. Burke, and M. Ernzerhof, Phys. Rev. Lett. **77**, 3865 (1996).

[37] G. Kresse and J. Hafner, Phys. Rev. B **47**, 558 (1993).

[38] P. E. Blochl, Phys. Rev. B **50**, 17953 (1994).

[39] G. Kresse and J. Furthmuller, Comput. Mater. Sci. **6**, 15 (1996).

[40] H. Mao1, C. Wang, H. E. Maynard-Casely, Q. Huang, Z. Wang, G. Cao, S. Li, and H. Luo, Europhys. Lett. **117**, 57005 (2017).

[41] Y. L. Page and P. Saxe, Phys. Rev. B **65**, 104104 (2002).

[42] G. Y. Guo and H. H. Wang, Chin. J. Phys. **38**, 949 (2000).

[43] K. R. Babu and G.-Y. Guo, Phys. Rev. B **99**, 104508 (2019).

[44] I. R. Shein and A. L. Ivanovskii, Tech. Phys. Lett. **35**, 961 (2009).

[45] R. Hill, Proc. Soc. London A **65**, 349 (1952).

[46] O. L. Anderson, J. Phys. Chem. Solids **24**, 909 (1963).

[47] P. Giannozzi, S. Baroni, N. Bonini, M. Calandra, R. Car, C. Cavazzoni, D. Ceresoli, G. L Chiarotti, M. Cococcioni, I. Dabo *et al.*, J. Phys.: Condens. Matter **21**, 395502 (2009).

[48] https://www.quantum-espresso.org/pseudopotentials.

[49] S. Baroni, S. de Gironcoli, A. Dal Corso, and P. Giannozzi, Rev. Mod. Phys. **73**, 515 (2001).

[50] W. L. McMillan, Phys. Rev. **167**, 331 (1968).

[51] P. B. Allen and R. C. Dynes, J. Phys. C **8**, L158 (1975).

[52] M. Born and K. Huang, *Dynamical Theory of Crystal Lattices* (Oxford University Press, Oxford, 1998).

[53] C. Kittel, *Introduction to Solid State Physics*, 8th ed. (Wiley, New Jersey, 2005).

[54] L. Boeri, O. V. Dolgov, and A. A. Golubov, Phys. Rev. Lett. **101**, 026403 (2008).

[55] J. M. Osorio-Guillen, S. I. Simak, Y. Wang, B. Johansson, and R. Ahuja, Solid State Commun. **123**, 257 (2002).

[56] M. Lei, J. L. Sarrao, W. M. Visscher, T. M. Bell, J. D. Thompson, A. Migliori, U. W. Welp, and B. W. Veal, Phys. Rev. B **47**, 6154 (1993).

[57] D. Kasinathan, A. Ormeci, K. Koch, U. Burkhardt, W. Schnelle, A. L. Jasper, and H. Rosner, New J. Phys. **11**, 025023 (2009).

[58] M. J. van Setten, S. Er, G. Brocks, R. A. de Groot, and G. A. de Wijs, Phys. Rev. B **79**, 125117 (2009).

[59] G. Wu, Y. L. Xie, H. Chen, M. Zhong, R. H. Liu, B. C. Shi, Q. J. Li, X. F. Wang, T. Wu, Y. J. Yan, J. J. Ying, and X. H. Chen, J. Phys.: Condens. Matter **21**, 142203 (2009).

[60] H. Takahashi, H. Soeda, M. Nukii, C. Kawashima, T. Nakanishi, S. Iimura, Y. Muraba, S. Matsuishi, and H. Hosono, Sci. Rep. **5**, 7829 (2015).

[61] F.-C. Hsu, J.-Y. Luo, K.-W. Yeh, T.-K. Chen, T.-W. Huang, P. M. Wu, Y.-C. Lee, Y.-L. Huang, Y.-Y. Chu, D.-C. Yan, and M.-K. Wu, Proc. Natl. Acad. Sci. USA **105**, 14262 (2008).

[62] J. H. Tapp, Z. Tang, B. Lv, K. Sasmal, B. Lorenz, P. C. W. Chu, and A. M. Guloy, Phys. Rev. B **78**, 060505(R) (2008).

[63] M. Rotter, M. Tegel, D. Johrendt, I. Schellenberg, W. Hermes, and R. Pottgen, Phys. Rev. B **78**, 020503(R) (2008).

[64] E. C. Stoner, Proc. R. Soc. London, Ser. A **169**, 339 (1939).

[65] J. F. Janak, Phys. Rev. B **16**, 255 (1977).

[66] G. Prando, Th. Hartmann, W. Schottenhamel, Z. Guguchia, S. Sanna, F. Ahn, I. Nekrasov, C. G. F. Blum, A. U. B. Wolter, S. Wurmehl, R. Khasanov, I. Eremin, and B. Buchner, Phys. Rev. Lett. **114**, 247004 (2015).

[67] S. Sen and H. Ghosh, Phys. Lett. A **379**, 843 (2015).

[68] D. J. Singh and M.-H. Du, Phys. Rev. Lett. **100**, 237003 (2008).

[69] G. Henkelman, A. Arnaldsson, and H. Jonsson, Comput. Mater. Sci. **36**, 354 (2006); E. Sanville, S. D. Kenny, R. Smith, and G. Henkelman, J. Comput. Chem. **28**, 899 (2007).

[70] M. Sunagawa, T. Ishiga, K. Tsubota, T. Jabuchi, J. Sonoyama, K. Iba, K. Kudo, M. Nohara, K. Ono, H. Kumigashira, T. Matsushita, M. Arita, K. Shimada, H. Na-matame, M. Taniguchi, T. Wakita, Y. Muraoka, and T. Yokoya, Sci. Rep. **4**, 4381 (2014).

[71] S. Sen and G.-Y. Guo, Phys. Rev. Mater. **4**, 104802 (2020).

[72] S. Grimme, J. Antony, S. Ehrlich, and S. Krieg, J. Chem. Phys. **132**, 154104 (2010).

[73] G. Y. Guo and W. M. Temmerman, Phys. Rev. B **41**, 6372 (1990).